BOUNDARY LAYER TRANSITION INDUCED BY DISTRIBUTED ROUGHNESS ARRAY

Qingqing Ye, Francesco Avallone, Daniele Ragni

Faculty of Aerospace Engineering
Delft University of Technology
Kluyverweg 1, 2629HS Delft, the Netherlands
q.ye-1@tudelft.nl, f.avallone@tudelft.nl, d.ragni@tudelft.nl

Meelan Choudhari

Computational AeroSciences Branch
NASA Langley Research Center
Hampton, VA 23681, USA
Meelan.M.Choudhari@nasa.gov

Damiano Casalino

Faculty of Aerospace Engineering
Delft University of Technology
Kluyverweg 1, 2629HS Delft, the Netherlands
d.casalino@tudelft.nl

ABSTRACT

The effects of a finite, spanwise-periodic array of cylindrical roughness elements on boundary layer transition over a NACA 0012 airfoil are investigated at a chord-based Reynolds number of 1.44×10^5 by using hotwire anemometry and infrared thermography. Both the number and the spanwise spacing of roughness elements in the array are varied in order to study their effect on the wake flow topology. Spanwise interaction between the roughness elements has an effect on the connection and the merging of neighbouring low-speed regions, which results in the formation of merged low-speed blobs (MLSs) that modify the spatial distribution and the amplitudes of the velocity streaks. When the spanwise distance between adjacent roughness elements equals 1.5 times the cylinder diameter, the transition location moves rapidly upstream. In this case, the two neighbouring low-speed regions overlap with each other in the near wake of the roughness, leading to the maximum growth in the velocity streak amplitude and the velocity fluctuations. The number of roughness elements affects the total number of MLSs within the boundary layer. For a single MLS behind a pair of cylinders, the Kelvin-Helmholtz instability dominates the growth of velocity fluctuations around the three-dimensional shear layers. When three cylinders are placed in the array, two MLSs appear in the near wake, which coalesce in to one low-speed blob downstream before the onset of transition, revealing the importance of Kelvin-Helmholtz instability.

INTRODUCTION

Understanding the role of surface roughness on transition has been a challenging topic until now. A widely accepted parameter to predict the effectiveness of a three-dimensional isolated roughness element on transition is the roughness-height-based Reynolds number, $Re_{kk} = u_k k/v$, where k is the height of roughness element, u_k is the unperturbed boundary layer velocity at height k, and v is the kinematic viscosity. The critical Re_{kk} for an isolated element refers to the value beyond which a rapid upstream shift in the transition onset location is observed. Three-dimensional roughness elements typically introduce a localized spanwise deflection of the streamlines within the mean boundary layer flow. One main feature detected downstream of the isolated roughness element corresponds to the counter-rotating pairs of streamwise vortices (Fransson et al. 2004), resulting in the formation of low- and high-speed streaks that modulate the boundary layer along both wall-normal and spanwise directions. If the streak amplitude exceeds a critical value, the flow can develop an unsteady streak instability, with either sinuous or varicose modulation of the streak structure, eventually resulting in a breakdown into turbulence (Andersson et al. 2001).

Due to increased geometric complexity, the study of distributed roughness effects presents more challenges than the case of an isolated three-dimensional roughness element. In the early experimental research, Von Doenhoff and Horton (1958) placed randomly distributed grit particles over a NACA 65-114 airfoil. When the largest grit particle from the group exceeds the critical value of Re_{kk} for an isolated roughness element, the transition location moves close to the grid location.

To further improve the current understanding of the transition process due to distributed surface roughness, other investigators have studied the roughness distributions that are spatially non-localised but fully deterministic in nature. For example, Muppidi and Mahesh (2012) studied the onset of transition in the presence of a sinusoidal roughness distribution in both streamwise and spanwise directions by using direct Navier-Stokes (DNS) simulations for a supersonic boundary layer (Ma = 2.9). Counter-rotating streamwise vortices were produced over the peaks in the roughness region. The vortices were found to gain strength along the length of the roughness patch via the interaction with the downstream peaks in the roughness height distribution. The strong streamwise vortices caused an unstable shear layer, which subsequently led to the onset of laminar-turbulent transition.

Although there has been much research on transition due to surface roughness on a flat plate, not all of which can be cited here due to space limitations, the effects of spanwise interaction between the various elements within a roughness distribution have not been investigated in a systematic manner, especially in a realistic aerospace application. In the present research, a single array of cylindrical roughness elements is placed on a NACA0012 airfoil to study the spanwise interaction between roughness elements. Infrared thermography and hotwire anemometry are used as diagnostic techniques to measure the surface temperature and flow velocity, respectively. The number and the spacing of roughness elements in the spanwise direction are varied to investigate their effects on the wake flow topology and the overall transition process.

EXPERIMENTAL SETUP AND FLOW CONDITIONS

Experiments were performed in the anechoic vertical open-jet wind tunnel (A-tunnel) of the Aerodynamics Laboratories of the Aerospace Engineering Faculty at the Delft University of Technology. The wind tunnel has a test section of 0.4×0.7 m^2 with a contraction ratio of 15:1. The maximum operating freestream velocity is 42.5 m/s, with a turbulence intensity below 0.1%. The freestream velocity distribution across the test section is uniform within 0.5%. A NACA0012 airfoil with 300 mm chord (c) and 400 mm span (s) (see Figure 1) was installed at zero degrees angle of attack, along the symmetry plane of the test section. A Cartesian system of coordinate axes centred at the leading edge of the airfoil is introduced, such that the x-axis is aligned with the airfoil chord, the z-axis is along the span, and the y-axis is normal to both of them.

A single array of cylindrical roughness elements with 4 mm diameter (d) and 1 mm height (k) was placed on one side of the airfoil surface. The centres of the roughness elements are located at $x_r = 0.21c$, i.e. downstream of the region of favourable pressure gradient. The number of roughness elements and the spanwise spacing (λ_z) in the array are summarized in Table 1. Experiments were performed at a freestream velocity of 7 m/s, corresponding to a chord Reynolds number ($Re_c = u_\infty c/v$) of 1.44×10^5. The measured boundary layer thickness (δ_{99}), displacement thickness (δ^*) and momentum thickness (θ) at the roughness location are 1.40, 0.47 and 0.18 mm, respectively. The ratio of roughness height and boundary layer thickness (k/δ_{99}) is 0.71, indicating that the roughness elements are fully submerged in the boundary layer. The corresponding value of Re_{kk} is equal to 500, which may be compared with the range of 140-515 that is considered to be critical for an isolated roughness element (Von Doenhoff and Braslow 1961)
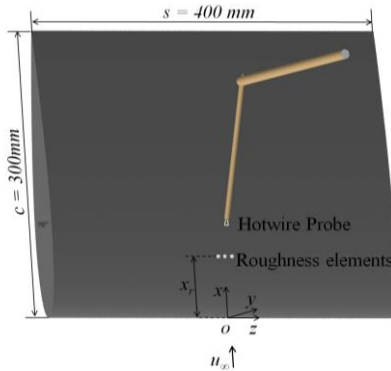

Figure 1. Sketch of hotwire setup.

Table 1. Roughness element distributions.

Distribution	Number of elements in the array	λ_z
Isolated cylinder	1	-
Single array	2	$2d$, $1.5d$
Single array	3	$1.5d$

The infrared (IR) thermography measurements were carried out with a CEDIP Titanium 530L IR system. The camera detector has a 320×256 pixels MCT (Mercury cadmium telluride) focal plane array. The sensor has a spectral response in the range of 7.7–9.3µm. An objective of 25mm focal length is mounted on the IR camera. The lens aperture is set to $f_\# = 2$. An integration time of 340µm was used in the experiment to achieve a satisfactory camera sensitivity. The recording frame rate was 200Hz at full resolution. The measurement domain extends from $x/c = 0.1$ until $x/c = 0.7$, resulting in a spatial resolution of approximately 1.74 pixels/mm. The surface of the model is heated with a high power daylight lamp to increase the temperature difference with the flow. The difference between the measured surface temperature T_s and the spanwise averaged temperature of the undisturbed laminar boundary layer $T_{s,bl}$ is non-dimensionalised with the latter temperature, as

$$T^* = (T_s (x, z) - T_{s, bl}(x))/ T_{s, bl}(x) \qquad (1)$$

As the model surface is preheated, the increase of convective heat transfer due to high local shear stress leads to a reduction in the measured surface temperature.

Velocity measurements behind the roughness elements were performed by using hotwire anemometry (HW) with a 5µm diameter single-wire probe (Dantec Dynamics P11). The hotwire probe was operated by a constant temperature bridge (TSI IFA-300), which has automatic adjustment of the overheat ratio. The development of the flow field is captured via five y-z cross-plane measurements downstream of the roughness elements. The sketch of the HW setup is shown in Figure 1. The movement of the hotwire probe is controlled by a computer-controlled traverse system with three degrees of freedom. The change of wall location at different x locations was taken into consideration to allow the measurement of the full boundary layer. The measurement data were acquired at a sampling frequency of 50kHz with a low-pass cut-off frequency of 20kHz. A sampling duration of 2s at each point ensured good statistical convergence.

ISOLATED CYLINDER

The flow topology around and downstream of an isolated cylindrical roughness element is discussed first in order to provide a baseline for the subsequent discussion of the interaction between multiple roughness elements and their effect on transition. The surface footprint of the cylinder is shown by the non-dimensionalised surface temperature distribution T^* in Figure 2, where $x_s = x - x_r$. A system of horseshoe vortices is formed in the region of flow separation just upstream of the cylinder. Previous literature indicates the presence of one to three counter-rotating spanwise vortex pairs in the region of flow separation within the $z = 0$ plane, depending on the Reynolds number and cylinder aspect ratio (Baker 1979). High values of shear stress are produced in the vicinity of the cylinder as a result of the spanwise vortices. The increased surface heat transfer is represented by a low-temperature region (dark grey, see Figure 2). The horseshoe vortices wrap around the upstream face of the cylinder and realign with the streamwise direction in the cylinder wake. The streamwise counter-rotating vortices are the major flow structures that modulate the boundary layer into low- and high-speed velocity streaks (Avallone et al. 2014, Fransson, et al. 2004, Ye et al. 2016). Crossplane contours of the streamwise velocity difference (u_d/u_∞), obtained by subtracting the time-averaged, undisturbed laminar boundary layer (u_{bl}/u_∞) from the time-averaged streamwise velocity (u/u_∞) in presence of the roughness, are shown in Figure 3(a) for selected streamwise locations ($x_s/d = 1.50, 3.75, 8.00, 11.50$ and 20.00). Contour lines of u/u_∞ are superimposed. At the first measurement station ($x_s/d = 1.50$), a central region of low-speed flow (referred to as 'CL') with a peak level of $-0.57u_\infty$ is formed as a result of flow separation behind the cylinder. Two sideward low-speed regions (referred to as 'SL') at $z/d = \pm0.75$ are attributed to the lateral upwash motion induced by the streamwise vortices from the horseshoe-vortex system. These streamwise vortices transport high momentum fluid toward the wall near the symmetry plane, leading to the formation of high-

speed regions (referred to as 'CH') near $z/d = \pm0.50$. At the intermediate wake station with $x_s/d = 3.75$, the magnitude of velocity deficit in the CL region is reduced considerably as the flow recovers from the separation behind the roughness element. Whereas the horseshoe vortices sustain the momentum transport and the velocity difference of SLs and CHs. At the farther downstream stations with $x_s/d = 8.00$ and $x_s/d = 11.50$, secondary sideward high-speed regions (referred to as 'SH') are formed on the outer sides of the SLs ($z/d = \pm1.00$ and 1.25 respectively), due to the formation of new streamwise counter-rotating vortex pairs (Ye, et al. 2016). The SHs induce additional low-speed regions (nSL, $z/d = \pm1.75$) at $x_s/d = 20.00$. The additional streamwise vortices and the induced high-speed regions move outward in the spanwise direction until $x_s/d = 25.00$, as shown in Figure 2. The high-speed regions remain at relatively constant spanwise positions until the end of the IR measurement domain.

The velocity fluctuations in the wake are studied next by plotting the root mean square (RMS) of the streamwise velocity fluctuations ($<u'>/u_\infty$) at $x_s/d = 1.50$, 3.75, 8.00, 11.50 and 20.00, as shown in Figure 3(b). Close to the cylinder ($x_s/d = 1.50$), the highest streamwise velocity fluctuations are produced at the top part of the shear layer surrounding the central low-speed region (CL), where the velocity profile is highly inflectional. The fact that the location of highest velocity fluctuations is closely aligned with the inflectional behaviour of the basic state profile indicates the growth of Kelvin-Helmholtz (K-H) instability at the wall-normal shear layer (Ergin and White 2006, Iyer and Mahesh 2013, Ye, et al. 2016). Since the velocity deficit in the CL region persists far downstream of the

roughness location, the inflectional instability at the wall-normal shear layer of CL sustains the production of velocity fluctuations until the most downstream measurement station ($x_s/d = 20.00$). At $x_s/d = 3.75$, 8.00 and 11.50, the high velocity deficit at SLs leads to the production of disturbances around the local shear layer. As a result, the active area of high intensity velocity fluctuations region increases in the spanwise direction. At the most downstream station $x_s/d = 20.00$, a more homogeneous distribution of velocity fluctuations can be observed over the entire wake. Penetration of high intensity fluctuations to the near wall region indicates the transitional behaviour of the flow.
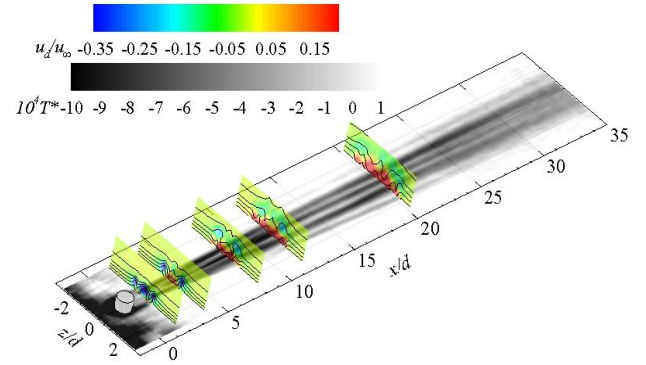

Figure 2. Surface temperature distribution around an isolated roughness element, superimposed by cross-plane contours of streamwise velocity difference (u_d/u_∞). Distances along the y axis are scaled by a factor of 3 for better visualization.
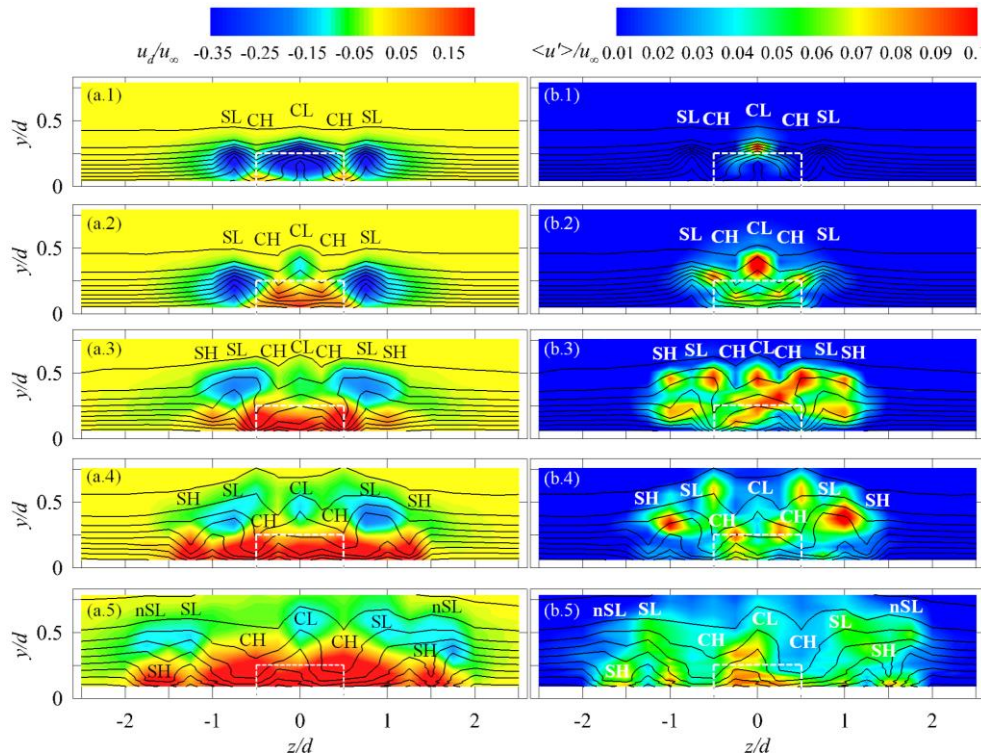

Figure 3. Cross-plane contours of streamwise velocity difference (u_d/u_∞) (a) and streamwise velocity fluctuations ($<u'>/u_\infty$) (b) in the wake of isolated roughness element. Black lines indicate contour lines of non-dimensional time-averaged velocity u/u_∞ with an increment of 0.1. (1)-(5) correspond to $x_s/d = 1.50$, 3.75, 8.00, 11.50 and 20.00. CL and SL indicate central and sideward regions of low-speed flow, CH and SH indicate central and sideward regions of high-speed flow. Distances along the y axis are scaled by a factor of 2 for better visualization.

SINGLE ARRAY WITH A PAIR OF CYLINDERS

Two pairs of cylinders with spanwise intervals of $\lambda_z = 2d$ and $\lambda_z = 1.5d$, respectively, were tested to examine the spanwise interaction between the wakes behind neighbouring roughness elements and the effect of λ_z on the flow topology. The cross-plane contours of streamwise velocity difference (u_d/u_∞) and RMS ($<u'>/u_\infty$) of streamwise velocity fluctuations

at five streamwise locations ($x_s/d = 1.50$, 3.75, 8.00, 11.50 and 20.00) for the two values of λ_z are shown in Figure 4 and Figure 5, respectively.

For $\lambda_z = 2d$ (Figure 4), the interaction between the wakes of the two cylinders begins at $x_s/d = 1.50$, where the interference between the SLs can be observed near $z/d = \pm0.20$. At $x_s/d = 3.75$, the two SL regions merge into one low-speed blob (MLS)

with a peak velocity deficit of $u_{d,min}/u_\infty$ = -0.55 along the symmetry plane. The two CLs connect with the MLS at this streamwise station, enhancing the velocity deficit of the MLS. At the downstream locations x_s/d = 8.00 and x_s/d = 11.50, the MLS lifts up from y/d = 0.2 to y/d = 0.5 due to the upwash motion and its velocity deficit decays with respect to the previous measurement station. At x_s/d = 20, the CLs and MLS fully combine into a single low-speed region close to the symmetry plane, with a more uniform distribution of the velocity fluctuations. Additionally, a homogenous high-speed region is formed near the wall, corresponding to an increased wall shear stress that is also accompanied by high intensity velocity fluctuations. The λ_z = 2d case shows higher levels of velocity fluctuations around the wall-normal and spanwise shear layers of the MLS than the fluctuations near the CLs and SLs (see Figure 4(b.3-b.5)). Two local maxima of the RMS of the velocity fluctuations are observed at the two nSLs at x_s/d = 20.00 (Figure 4(b.5)). The unsteady disturbances produced at

nSLs possibly contribute to the lateral growth of the wake (Kuester and White 2016, Ye, et al. 2016).

For the smaller λ_z = 1.5d (Figure 5), the closer proximity between the neighbouring cylinders promotes earlier merging of the SLs, right behind the cylinders at x_s/d = 1.50, which now shows a higher velocity deficit ($u_{d,min}/u_\infty$ = -0.72) with respect to the previous configurations. The MLS undergoes a faster lift up as a result of the stronger low-speed region and a higher upwash. The CLs behind each cylinder quickly merge with the MLS, causing the merged region to exhibit a high velocity deficit until x_s/d = 20.00. The two high-speed regions close to the wall are connected to each other but are not completely merged. The wake is symmetric with respect to the centre plane at all streamwise stations. The MLS and the induced inflection velocity profile lead to the growth of instability and a higher level of velocity fluctuations at the surrounding shear layer than the fluctuation levels near the SLs.
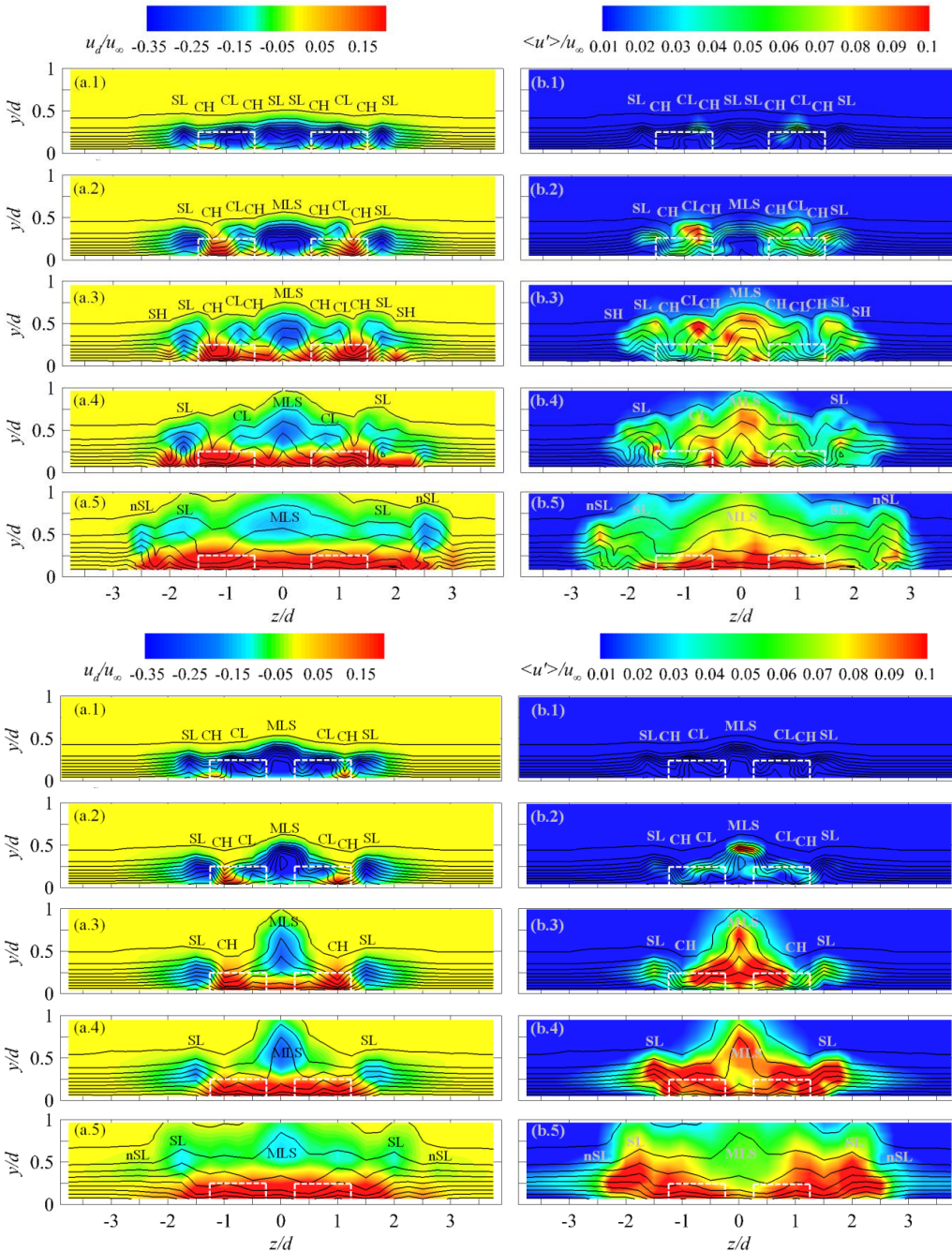

Figure 4. Cross-plane contours of streamwise velocity difference (u_d/u_∞) (a) and streamwise velocity fluctuations ($<u'>/u_\infty$) (b) in the wake of a single array with two cylinders for λ_z = 2d. Black lines are contour lines of non-dimensional time-averaged velocity u/u_∞ with an increment of 0.1. (1)-(5) correspond to x_s/d = 1.50, 3.75, 8.00, 11.50 and 20.00. MLS, CL and SL indicate merged, central, and sideward regions of low-speed flow, CH and SH indicate central and sideward regions of high-speed flow. Distances along the y axis are scaled by a factor of 2 for better visualization.

Figure 5. Cross-plane contours of streamwise velocity difference (u_d/u_∞) (a) and streamwise velocity fluctuations ($<u'>/u_\infty$) (b) in the wake of a single array with two cylinders for λ_z = 1.5d. Black lines are contour lines of non-dimensional, time-averaged velocity u/u_∞ with an increment of 0.1. (1)-(5) correspond to x_s/d = 1.50, 3.75, 8.00, 11.50 and 20.00. MLS, CL and SL indicate merged, central, and sideward regions of low-speed flow, CH and SH indicate central and sideward regions of high-speed flow. Distances along the y axis are scaled by a factor of 2 for better visualization.

The breakdown to turbulence behind isolated roughness elements is conventionally related to the formation and subsequent growth of a turbulent wedge. The inception of a turbulent wedge can be visualized via the surface temperature distribution behind the array of cylinders as shown in Figure 6. The streamwise location where the wake width begins to increase is identified as the transition location (Avallone et al. 2016, Zhong et al. 2003). For an isolated cylinder, the wake develops with a relatively constant width downstream of $x_s/d =$ 25.00, indicating a laminar condition throughout the domain of interest (see Figure 2). For the case $\lambda_z = 2d$, although the secondary low-temperature streaks (corresponding to SH) are already present at $x_s/d = 9.5$, the wake width remains constant in the downstream region. For two-cylinder configurations, the lateral propagation of the wake can be observed only for the smaller spanwise interval of $\lambda_z = 1.5d$, beginning at $x_s/d =$ 15.72, which is taken as the transition location.
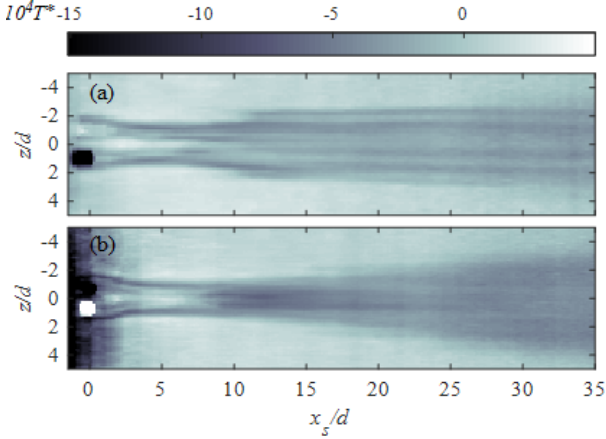

Figure 6. Surface temperature distribution behind a pair of cylinders. (a) corresponds to $\lambda_z = 2d$ and (b) to $\lambda_z = 1.5d$.

SINGLE ARRAY WITH THREE CYLINDERS

Increasing the number of roughness elements in the array add to the complexity of the interaction between the element wakes. In this section, three cylindrical roughness elements are placed in an array with spanwise intervals (λ_z) equal to 1.5d to study the effect of the number of elements on the transition process. The cross-plane contours of streamwise velocity difference (u_d/u_∞) and streamwise velocity fluctuations ($<u'>/u_\infty$) are shown in Figure 7 for $x_s/d = 1.50$, 3.75, 8.00, 11.50 and 20.00, respectively. The surface temperature distribution (T^*) is shown in Figure 8.

Similar to the case of two cylinders, the adjacent sideward low-speed regions (SL) connect and merge into a single low-speed region on both spanwise sides of the middle cylinder at the first two measurement stations ($x_s/d = 1.50$ and 3.75, Figure 7(a.1) and 7(a.2)). At $x_s/d = 3.75$, the maximum velocity deficit increases from $u_{d,min}/u_\infty = -0.76$ to -0.81 compared to the dual cylinder case. The CL at the wake centre exhibits a decrease in strength. The other CLs on the outer side of the spanwise region merge with MLSs. A remarkable decrease in the velocity fluctuations can be observed, which may be due to the interaction between the two neighbouring MLSs close to the symmetry plane. Farther downstream at $x_s/d = 8.00$ (Figure 7(a.3)(b.3)), the high velocity deficit associated with the MLSs contributes to the formation of local maxima in the velocity fluctuations within the surrounding shear layer. A high speed region is produced close to the symmetry plane ($z/d = 0$), corresponding to the central low-temperature region in Figure 8, which can be observed in the range $x_s/d = [0, 13.85]$ in the instantaneous surface temperature distribution. At the most downstream station $x_s/d = 20.00$, the two MLSs merge into one single low-speed blob, leading to a fully symmetric wake distribution. Furthermore, the wake width begins to increase downstream of $x_s/d = 20.48$, indicating the onset of transition (see Figure 8). Thus, even though the asymmetric disturbance first appear within the near wake, it decays before the inception of the turbulent wedge, and hence, this disturbance does not influence the onset of transition.

VARIATION IN STREAK AMPLITUDE

The amplitude of spanwise modulation caused by the presence of the roughness elements can be characterized through the streak amplitude (A_u), defined as:

$$A_u(x) = \frac{1}{2}[\max_{y,z}(u_d(x,y,z)/u_\infty) - \min_{y,z}(u_d(x,y,z)/u_\infty)] \quad (2)$$

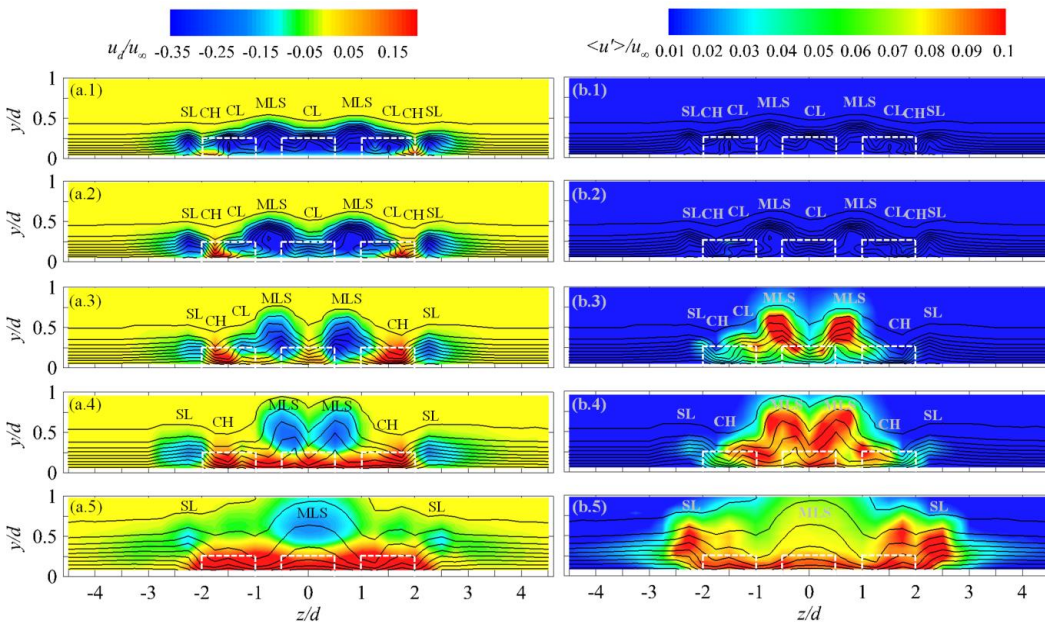Figure 7. Cross-plane contours of streamwise velocity difference (u_d/u_∞) (a) and streamwise velocity fluctuations ($<u'>/u_\infty$) (b) in the wake of single array with three cylinders for $\lambda_z = 1.5d$. Black lines are contour lines of non-dimensional time-averaged velocity u/u_∞ with an increment of 0.1. (1)-(5) correspond to $x_s/d = 1.50$, 3.75, 8.00, 11.50 and 20.00. MLS, CL and SL indicate merged, central and sideward regions of low-speed flow, CH and SH indicate central and sideward regions of high-speed flow. Distances along the y axis are scaled by a factor of 2 for better visualization.

For an isolated cylinder (Figure 9), A_u has a maximum value of 0.34 and its variation across all measurement stations is small. The wake interactions behind a pair of cylinders cause A_u to increase for both $\lambda_z = 2d$ and $1.5d$. The maximum amplitude $A_{u,max}$ is reached near $x_s/d = 3.75$, followed by a steep reduction up to the same value of A_u as that measured behind an isolated cylinder. The reduction in A_u behind two cylinders is attributed to a more pronounced spanwise mixing of the wakes. Increasing the number of roughness elements, the streak amplitude reaches comparable level with the double cylinder case for $\lambda_z = 1.5d$. The main difference of A_u happens at the intermediate measurement stations $x_s/d = 3.75$ and 8.00, reaching higher magnitude. Transition is promoted when the velocity streak amplitude reaches a certain level ($A_u > 0.45$) close to the cylinder (case $\lambda_z = 1.5d$). The induced velocity fluctuations due to K-H instability are intensified at the location of MLS. When the streak amplitude is smaller than the critical value ($A_u < 0.45$ for $\lambda_z = 2d$), the velocity fluctuations produced in the wake remain comparable to those in the isolated roughness case, which cannot lead to transition.
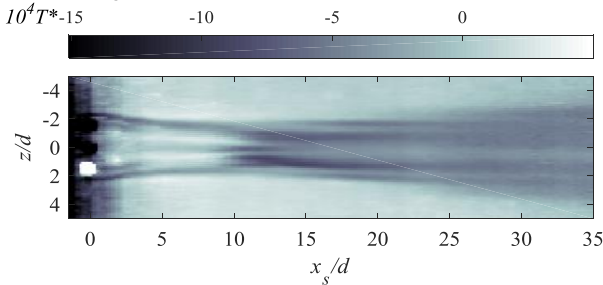

Figure 8. Surface temperature distribution behind a single array with three cylinders, $\lambda_z = 1.5d$.
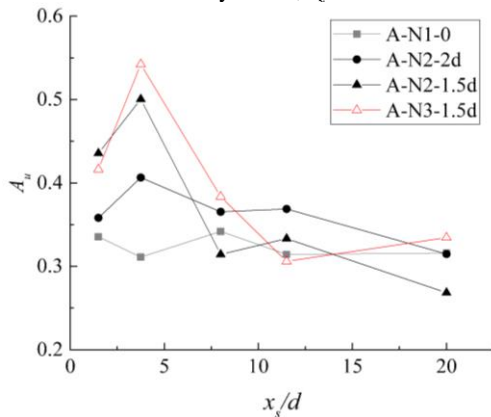

Figure 9. Streak amplitude (A_u) behind isolated cylinder and single cylinder array, A: single array, N: number of cylinders in the first array, the last column is the spanwise interval (λ_z).

CONCLUSION

The transitional flow features over a spanwise periodic array of cylindrical roughness elements have been investigated experimentally to reveal the effect of roughness interaction on transition. The roughness elements are placed on a NACA 0012 airfoil at a chord-based Reynolds number of 1.44×10^5. The velocity and temperature field are measured by hotwire anemometry and infrared thermography, respectively. The number and the spacing of roughness elements in the spanwise direction are varied to investigate their effects on the wake flow topology as well as the overall transition process.

An isolated roughness element induces three low-speed regions in the wake. The spanwise interaction between multiple roughness elements involves the connection and merging of the neighbouring low-speed regions close to or at the roughness location, leading to the formation of stronger low-speed blobs (MLS) within the wake. For the case of a pair of cylinders with $\lambda_z = 2d$, the increase of streak amplitude is relatively low, yielding a trivial effect on the overall transition process. For the case $\lambda_z = 1.5d$, however, two neighbouring low-speed regions overlap in the vicinity of the roughness. The merged central low-speed region leads to the growth of unsteady, Kelvin-Helmholtz disturbances within the surrounding three-dimensional shear layer and promotes the transition to turbulence.

When three cylinders interact with each other, two additional, merged, low-speed regions form on each side of the central cylinder. The merged low-speed regions coalesce, leading to a single low-speed blob and a fully symmetrical wake distribution before the onset of transition. Similar to the case of cylinder pair, the transition to turbulence is induced by Kelvin-Helmholtz instability.

REFERENCES

Andersson, P., Brandt, L., Bottaro, A., Henningson, D. S., 2001, "On the breakdown of boundary layer streaks". *Journal of Fluid Mechanics,* Vol. 428, pp. 29-60.

Avallone, F., Schrijer, F. F. J., Cardone, G., 2016, "Infrared thermography of transition due to isolated roughness elements in hypersonic flows". *Physics of Fluids,* Vol. 28, pp. 024106.

Avallone, F., Ye, Q., Schrijer, F. F. J., Scarano, F., Cardone, G., 2014, "Tomographic PIV investigation of roughness-induced transition in a hypersonic boundary layer". *Experiments in Fluids,* Vol. 55, pp. 1852.

Baker, C. J., 1979, "The laminar horseshoe vortex". *Journal of Fluid Mechanics,* Vol. 95, pp. 347-367.

Ergin, F. G., White, E. B., 2006, "Unsteady and transitional flows behind roughness elements". *AIAA Journal,* Vol. 44, pp. 2504-2514.

Fransson, J. H. M., Brandt, L., Talamelli, A., Cossu, C., 2004, "Experimental and theoretical investigation of the nonmodal growth of steady streaks in a flat plate boundary layer". *Physics of Fluids,* Vol. 16, pp. 3627-3638.

Iyer, P. S., Mahesh, K., 2013, "High-speed boundary-layer transition induced by a discrete roughness element". *Journal of Fluid Mechanics,* Vol. 729, pp. 524-562.

Kuester, M. S., White, E. B., 2016, "Structure of turbulent wedges created by isolated surface roughness". *Experiments in Fluids,* Vol. 57, pp. 47.

Muppidi, S., Mahesh, K., 2012, "Direct numerical simulations of roughness-induced transition in supersonic boundary layers". *Journal of Fluid Mechanics,* Vol. 693, pp. 28-56.

Von Doenhoff, A. E., Braslow, A. L., 1961, "The effect of distributed surface roughness on laminar flow". In: Lachmann, G. V. (ed) Boundary Layer and Flow Control. *Pergamon*, pp. 657-681.

Von Doenhoff, A. E., Horton, E. A., 1958, "A low-speed experimental investigation of the effect of a sandpaper type of roughness on boundary-layer transition". NACA-TN-3858.

Ye, Q., Schrijer, F. F. J., Scarano, F., 2016, "Geometry effect of isolated roughness on boundary layer transition investigated by tomographic PIV". *International Journal of Heat and Fluid Flow,* Vol. 61, pp. 31-44.

Zhong, S., Chong, T. P., Hodson, H. P., 2003, "A comparison of spreading angles of turbulent wedges in velocity and thermal boundary layers". *Journal of Fluids Engineering,* Vol. 125, pp. 8.